

OPTICAL TOMOGRAPHY

PACS numbers: 87.57.–s; 42.30.Wb; 87.64.Cc; 78.67.Bf
DOI: 10.1070/QE2010v040n06ABEH014294

Nanoparticles as contrast-enhancing agents in optical coherence tomography imaging of the structural components of skin: Quantitative evaluation

M.Yu. Kirillin, P.D. Agrba, M.A. Sirotkina, M.V. Shirmanova, E.V. Zagainova, V.A. Kamensky

***Abstract*. This work examines the effect of gold nanoshells and titania nanoparticles on the imaging contrast of structural components of skin in optical coherence tomography (OCT). Experimental data are compared to Monte Carlo (MC) simulation results. In experiments with pig skin *in vivo*, the epidermis – dermis contrast is improved from 0.78 ± 0.03 to 0.92 ± 0.04 by gold nanoshells applied to the skin surface and from 0.78 ± 0.03 to 0.86 ± 0.04 by titania nanoparticles. The contrast of glands is enhanced by titania from 0.68 ± 0.12 to 0.84 ± 0.07. The highest contrast is reached 120 – 150 min after applying gold nanoshells and 160 – 200 min after applying titania. According to the MC simulation results, the contrast of inclusions increases from zero to 0.85 and 0.65, respectively.**

Keywords: *optical coherence tomography, nanoparticles, imaging contrast, Monte Carlo simulation.*

1. Introduction

The rapid progress in optical techniques for probing the internal structure of various objects is accompanied by wide application of such techniques in biomedical diagnostics [1 – 4]. Conventional techniques for imaging the internal structure of biological tissue, such as X-ray computed tomography [5] and magnetic resonance tomography [6], provide images with a spatial resolution no better than 100 – 1000 μm [5, 6], which is often insufficient to identify pathologies. Moreover, the use of X-ray tomography is limited by the adverse effect of ionising radiation on living organisms. Recent years have seen successful attempts to bring the spatial resolution of optical techniques to the cell level (~ 10 μm). In particular, this can be achieved using confocal optical microscopy [7] and optical coherence tomography (OCT) [8, 9].

Built upon the low-coherence interferometry principle, OCT offers the advantages of high-speed imaging, ease of implementation, compact design and instrumental reliability. OCT imaging of covering tissues – skin and mucosas – has been extensively described in the literature [10]. Unfortunately, one serious drawback to OCT in skin imaging is the small imaging depth (less than 1.5 mm) and low contrast [10] because of the strong scattering of probe radiation.

Light scattering in biological tissues is caused by the nonuniform refractive index distribution and depends on the structure of the tissue. The index distribution in turn determines macroscopic optical parameters: the scattering coefficient μ_s, absorption coefficient μ_a and anisotropy factor g. Varying the refractive index distribution in biological tissue, e.g., using compression [10, 11], clearing agents [1] or contrast agents [12 – 15], one can control its optical characteristics. In a number of studies, nanoparticles were used as OCT contrast agents [12 – 16]. When applied to the skin surface, they penetrate into the tissue and, owing to their more isotropic phase function in comparison with the scattering components of skin, increase probe radiation backscattering [12 – 15]. The increased backscattering by structural components containing higher nanoparticle concentrations in comparison with surrounding tissues enhances OCT imaging contrast.

Recent work [12, 15] has shown that OCT can be used to visualise accumulations of gold nanoshells in skin. However, OCT contrast enhancement through *in vivo* administration of nanometre-sized agents has not been quantified in those studies.

In this paper, we present experimental studies and Monte Carlo simulations aimed at quantifying the effect of gold nanoshells and titania nanoparticles as contrast-enhancing agents in OCT imaging of pig skin.

2. Materials and methods

2.1 Imaging subject

Pig skin was chosen for imaging because it is similar in structure and thickness to human skin and has a high density of structural inhomogeneities.

Figure 1 schematically illustrates the structure of pig skin. It has a multilayer structure and comprises epidermis, consisting of the outermost, horny layer (stratum corneum) and cell layers, and dermis. The dermis can be divided into upper dermis, containing hair follicles and gland ducts, and lower dermis, containing sebaceous glands.

M.Yu. Kirillin, P.D. Agrba, V.A. Kamensky Institute of Applied Physics, Russian Academy of Sciences, ul. Ulyanova 46, 603950 Nizhnii Novgorod, Russia; e-mail: mkirillin@yandex.ru, agrbapd@gmail.com;
M.A. Sirotkina, M.V. Shirmanova, E.V. Zagainova Nizhnii Novgorod State Medical Academy, pl. Minina i Pozharskogo 10/1, 603005 Nizhnii Novgorod, Russia; e-mail: sirotkina_m@mail.ru, shirmanovam@mail.ru

Received 10 February 2010; revision received 11 May 2010
Kvantovaya Elektronika **40** (6) 525 – 530 (2010)
Translated by O.M. Tsarev

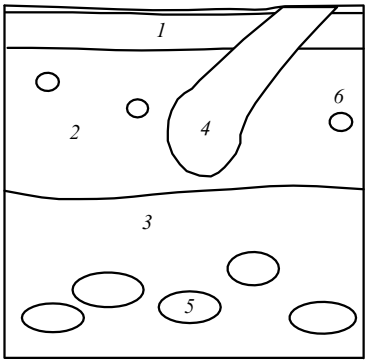

Figure 1. Schematic of the pig skin structure: (*1*) epidermis; (*2*) upper dermis; (*3*) lower dermis; (*4*) hair follicle; (*5*) glands; (*6*) ducts.

2.2 Nanoparticles

We studied two types of particles: gold nanoshells (produced at the Institute of Biochemistry and Physiology of Plants and Microorganisms, Russian Academy of Sciences) and titania in the form of aqueous suspension. The silica core radius and gold shell thickness were 75 and 25 nm, respectively [13]. The titania nanoparticles (Promkhim Group) consisted of high-purity (99.999 %) rutile and were 108 ± 24 nm in diameter. When suspended in water, the nanoparticles were highly aggregated, with an average aggregate size of 400 nm. To break down the aggregates and prevent aggregation, the nanoparticles were sonicated for 30 min before use.

2.3 Experimental procedure

Our experiments were performed with an optical coherence tomograph designed at the Institute of Applied Physics, Russian Academy of Sciences [17]. The centre wavelength of the probe radiation was 910 nm, and the source bandwidth was ~ 50 nm. The axial resolution in air was 15 μm, and the transverse resolution was 20 μm. The probe diameter was 2.7 mm, and the OCT image acquisition time was 5 s.

During image acquisition, the probe was pressed against the skin surface with a constant load in order to minimise compression variations, which otherwise might have obscured the variations in OCT images after the application of nanoparticles. Prior to *in vivo* experiments, the hair was removed from the skin surface. To obtain a reference image and separate the effects related to nanoparticles from wetting effects, distilled water was applied to a neighbouring skin area. OCT images were obtained 15 min after applying the agents and then every 30 min over a period of 5 h. At each time point, 15–20 images were collected from a 1 cm^2 area.

After each experiment, a skin biopsy was done (under local anaesthesia). The structural components of skin in OCT images were identified by comparing them with appropriate histological images [12, 13]. The presence of nanoparticles in the skin was checked by electron microscopy [13].

2.4 Monte Carlo simulation

Monte Carlo (MC) simulation of light propagation in a scattering medium involves multiple calculations of random photon paths in the medium and subsequent statistical analysis of the results. The input parameters are the optical properties and geometry of the medium, which determine the length and shape of individual photon paths.

OCT signals and images were simulated using a code written and tested earlier [18–20]. The speckle structure of the images was left out of consideration, which allowed us to generate model images with a larger signal-to-noise ratio. In computations, we used the Henyey–Greenstein phase function, widely employed in MC simulation of light propagation in biological tissues, including skin [21]:

$$f_{\mathrm{HG}}(\theta) = \frac{1}{4\pi} \frac{1 - g^2}{(1 + g^2 - 2g\cos\theta)^{3/2}}, \quad (1)$$

where θ is the scattering angle and g is the anisotropy factor.

Two-dimensional (2D) OCT images can be generated by successively simulating 1D OCT signals (A-scans) with a particular step between probing points. The step is usually equal to the half-amplitude probe beam diameter, which corresponds to experimental OCT image collection conditions.

The parameters used in our simulations were similar to those of the OCT system. The coherence length, l_{coh}, was taken to be 15 μm. 2D OCT images were simulated by computing 50 successive A-scans with a scan step of 20 μm. Each A-scan simulation included 5×10^6 photons. The computation time per OCT image (Intel Pentium 4, clock speed of 2.8 GHz) was ~ 10 h.

Figure 2 schematically illustrates the four-layer skin model deduced from experimental OCT images. The optical parameters were obtained by averaging those of human skin (Table 1) [21, 22].

In examining epidermis–dermis contrast enhancement, nanoparticles were thought to be present in the stratum corneum and epidermis. In simulating the imaging contrast of structural features in the skin, the upper dermis was assumed to contain a 0.10-mm-radius spherical hair follicle,

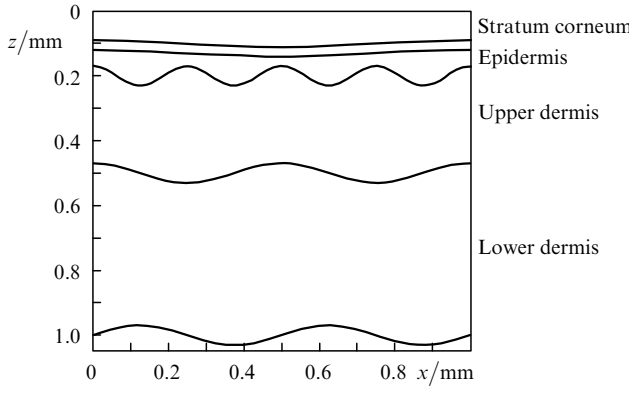

Figure 2. Four-layer skin model used in MC simulation.

Table 1. Optical properties of the skin layers ($\lambda = 910$ nm).

No.	Layer	h/mm	μ_s/mm^{-1}	μ_a/mm^{-1}	g	N
1	Stratum corneum	0.03	35	0.02	0.9	1.45
2	Epidermis	0.07	12	0.1	0.9	1.39
3	Upper dermis	0.3	7	0.7	0.85	1.4
4	Lower dermis	0.5	12	0.1	0.9	1.4

Note: h is the skin thickness; N is the refractive index.

with no nanoparticles, and nanoparticles were placed in the three upper layers.

Simulations were performed for two types of nanoparticles: gold nanoshells and titania particles identical in parameters to those used in our experiments. The complex refractive indices of silica, gold and titania at 910 nm were assessed from earlier data [23–25]. The scattering cross sections of the gold nanoshells and titania particles were 0.070 and 6.90×10^{-5} μm^2, and their absorption cross sections were 0.008 and 1.65×10^{-5} μm^2, respectively. Since the nanoparticle concentration in skin was difficult to determine with sufficient accuracy in our experiments, the volume fraction of gold nanoshells was varied in the simulations from 0.001 % to 0.01 %, and that of titania nanoparticles, from 0.01 % to 0.5 %.

2.5 OCT contrast evaluation procedure

To quantify the effect of nanoparticles on the optical properties of the layers, we used the concept of OCT imaging contrast. The contrast was evaluated as follows: An area homogeneous along the transverse coordinate was selected in the tomogram (Fig. 3a), the OCT signal was averaged over the transverse coordinate within this area, and the signal intensity was plotted against depth (averaged A-scan). Next, we determined the intensities (in decibels) of the layers of interest in the OCT image (Fig. 3b) and their difference (intensity ratio).

The contrast of inclusions in OCT images was evaluated as the change in the contrast of their upper boundary because diffusing nanoparticles predominantly deposited on it.

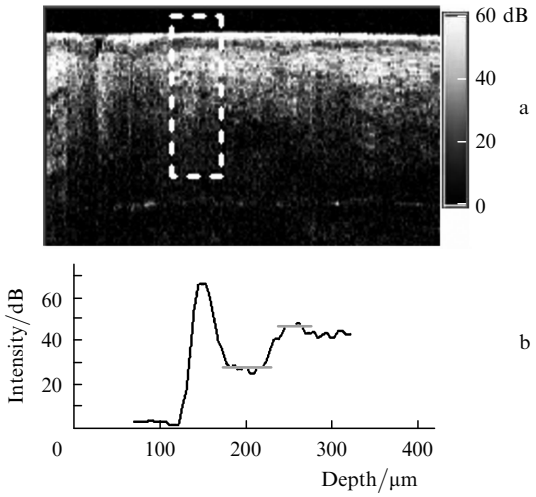

Figure 3. Evaluation of the contrast between layers in OCT images: (a) area homogeneous in the transverse direction in the OCT image; (b) OCT signal averaged over the transverse coordinate within this area (A-scan). The horizontal markers indicate the intensities (in decibels) corresponding to the layers of interest, the difference between which is contrast.

3. Results and discussion

3.1 Experimental data

According to our earlier results, nanoparticles increase the contrast of epidermis and glands. The maximum accumulation time depends on the type of nanoparticle: 150 min for gold nanoshells and 180 min for titania nanoparticles [20]. Figure 4 shows typical OCT images of pig skin without nanoparticles and at the instant of maximum nanoparticle accumulation.

The OCT images collected 150 min after applying gold nanoparticles and 180 min after applying titania demonstrate that their OCT signal considerably exceeds that in the reference image. This suggests that the nanoparticles penetrating into the skin increase backscattering at all depths. As a result, the OCT imaging depth for skin increases, and inclusions with a low OCT signal level (glands located at considerable depths) are better seen (Fig. 4).

The A-scans averaged over the transverse coordinate, obtained from the OCT images of skin in Fig. 4, are presented in Fig. 5. The dashed lines represent the A-scans of the skin with no nanoparticles, and the solid lines represent the A-scans performed after applying titania and gold nanoparticles.

In the OCT images collected before applying nanoparticles, the epidermis–dermis contrast was 0.78 ± 0.03. Just after the titania nanoparticle suspension was applied, the contrast dropped to 0.60 ± 0.09 (Fig. 6a). One possible reason for this is that the nanoparticles penetrate into the epidermis, increasing backscattering by this layer. Subsequently, the contrast increases and remains at a level of 0.86 ± 0.04 between 120 and 240 min after applying the particles. The likely reason for this is that the nanoparticles pass from the epidermis to the dermis. The contrast then gradually decreases, reaching 0.81 ± 0.04 300 min after the suspension was applied.

After applying gold nanoshells, the epidermis–dermis contrast slightly increases over time, from 0.78 ± 0.03 to 0.92 ± 0.04, reaching the maximum level after 120–150 min

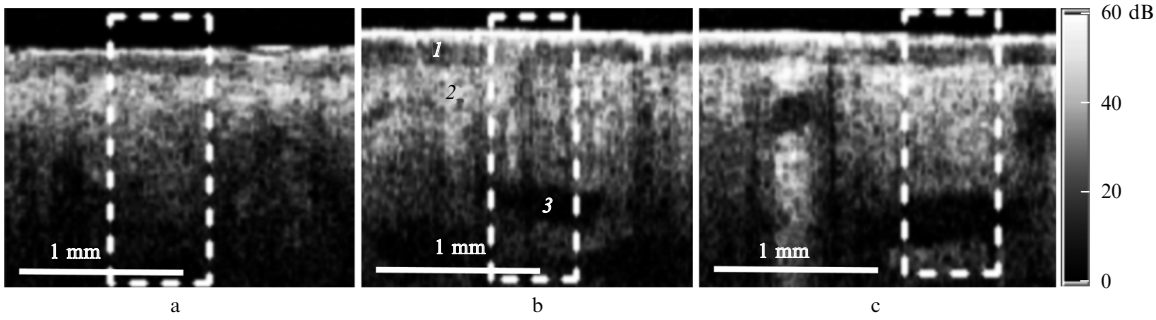

Figure 4. *In vivo* OCT images of pig skin (a) without nanoparticles (reference image), (b) 150 min after applying gold nanoparticles and (c) 180 min after applying titania. The dashed lines delineate the transverse averaging area; (*1*) epidermis, (*2*) dermis, (*3*) inclusion.

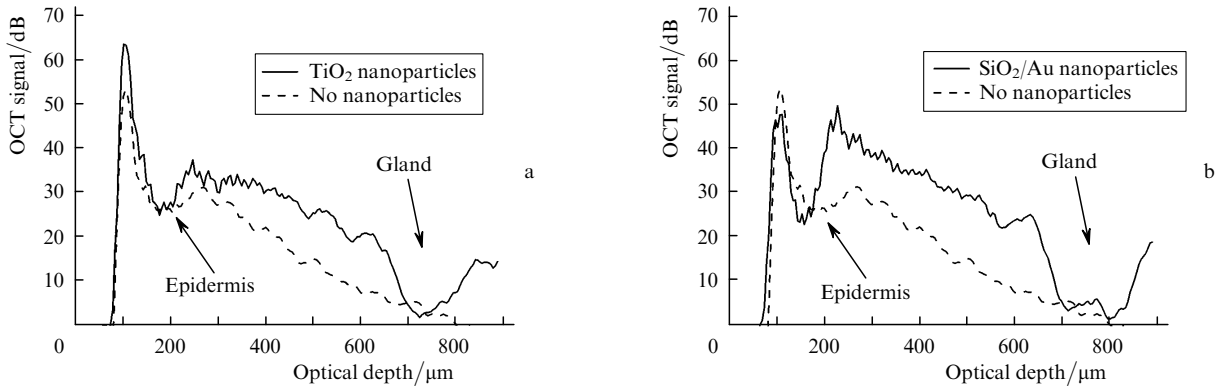

Figure 5. Averaged A-scans of pig skin (a) 180 min after applying a titania suspension and (b) 150 min after applying a gold nanoshell suspension. The averaging areas are delineated by dashed lines in Fig. 4.

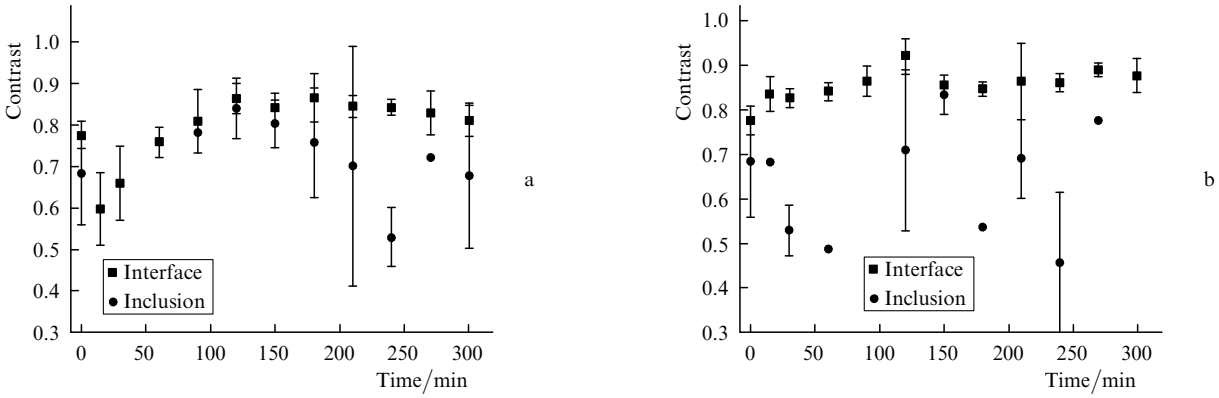

Figure 6. Variation of the epidermis–dermis contrast and the contrast of glands after applying (a) a titania nanoparticle suspension and (b) gold nanoshells to the skin surface.

and varying around 0.87 thereafter (Fig. 6b). The epidermis-dermis contrast in this case is seen to remain unchanged during the first few minutes after applying the nanoshells. This may be because gold particles pass through the epidermis more rapidly than do titania particles.

The time dependence of the contrast between inclusions and the surrounding dermis layers in the presence of gold nanoparticles shows no systematic variation. Moreover, the uncertainty in our contrast measurements is too high to draw definite conclusions as to the effect of gold nanoparticles on the contrast of inclusions. This is due to the small number of inclusions in the OCT images obtained with gold nanoparticles.

3.2 Monte Carlo simulation

To interpret the above results in greater detail, we performed Monte Carlo simulation of the contrast of inclusions and the epidermis–dermis contrast. The OCT images obtained by the MC method are presented in Fig. 7. The OCT signal intensity is also given in decibels.

The inclusions were thought to be indistinguishable from the surrounding tissue by OCT with no contrast agents. For this reason, the simulated OCT image is multilayer, each layer being uniform in structure (Fig. 7a). In simulations of biological tissue in the presence of nanoparticles, these were taken to be evenly distributed in the three upper layers, except for the inclusion. The volume fractions of gold nanoshells and titania particles were 0.01 % and 0.5 %, respectively (Figs 7b, 7c).

The simulated and experimental OCT images of the tissue with no nanoshells (Figs 7a and 4a, respectively) have a longitudinal structure, with the signal intensity decreasing steadily with increasing depth within each layer. The experimental image has axial inhomogeneities, related to

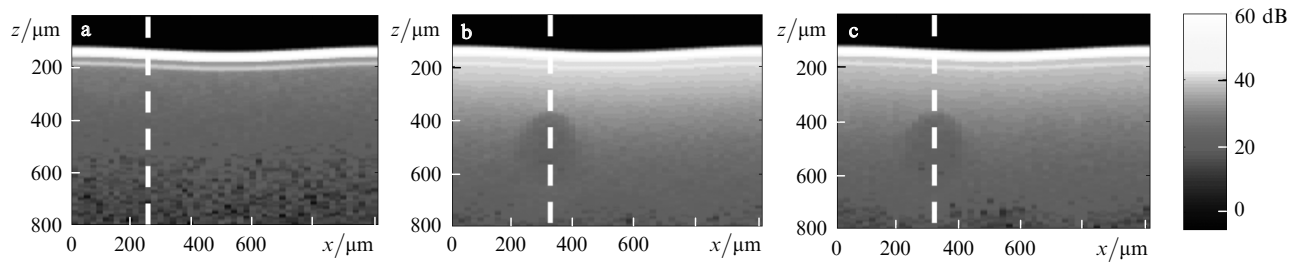

Figure 7. OCT images of skin obtained by MC simulation: (a) no nanoparticles (reference image); (b) gold nanoshells (0.01 vol %) and (c) titania particles (0.5 vol %) in the three upper layers. The hair follicle is assumed to be in the upper dermis.

specific features in the structure of the tissue. These features were left out of account in the simulation because they produce no qualitative changes in the effect under consideration. In addition, the distinctions between the simulated and experimental images may be due to the fact that the average optical parameters used in the simulation differed from the optical parameters of the tissue studied. Yet another noteworthy feature of the model is that the optical parameters of inclusions are identical to those of the layer they are embedded in. For this reason, the inclusions are not seen (zero contrast) in the simulated OCT images of the tissue with no nanoparticles. At the same time, the inclusions are seen in the experimental OCT images of the tissue. In the simulated OCT images of the tissue containing nanoparticles (Fig. 7b), the inclusion is seen, indicating an increase in contrast, in accordance with experimental data. The distinctions in this case may result from the fact that, in our experiments, the nanoparticles penetrate into the skin from its surface, their depth profile is thus nonuniform, and they penetrate as well into the inclusion. Moreover, there is a sharp change in concentration across the interface between regions differing in diffusion properties, which leads, in particular, to an increase in epidermis–dermis contrast. In the simulation, the gold nanoshells were evenly distributed throughout the tissue (except for the inclusion), which led to a higher contrast of the inclusion in comparison with the experiments, but their was no epidermis–dermis contrast.

Figure 8 shows A-scans averaged over the transverse coordinate, derived from the MC OCT images. The dashed lines represent the A-scans of the skin with no nanoparticles, and the solid lines represent those performed after applying titania and gold nanoparticles. Like in the *in vivo* experiments, both the gold nanoshells and titania increase the backscattering intensity at all depths and the contrast of inclusions.

Figure 9 shows the simulated epidermis–dermis contrast and contrast of inclusions as functions of the volume fraction of nanoparticles in the skin. Increasing the volume fraction of gold nanoparticles from 0 to 0.5 % increases the contrast of the inclusion from 0 to 0.6 and the epidermis–dermis contrast from 0.2 to 0.6. A similar increase in the volume fraction of titania particles is accompanied by an increase in contrast from 0 to 0.65 and from 0.25 to 0.75, respectively.

The MC simulation results are in qualitative agreement with the *in vivo* imaging data, suggesting that the model used adequately represents the system, but the quantitative changes in imaging contrast in the OCT of the tissue differ markedly. One possible origin of the discrepancy between the experimental and MC simulation data is that the inclusions were taken to be unseen in the simulated OCT images (the optical parameters of the inclusions were identical to those of the layer they were embedded in) of the tissue containing no nanoparticles. However, the inclusions were seen in the experimental OCT images before applying nanoparticles, even though with lower contrast than in the presence of nanoparticles. Moreover, the nanoparticles were taken to be evenly distributed throughout the upper layers in the simulation, in contrast to what took place in our experiments.

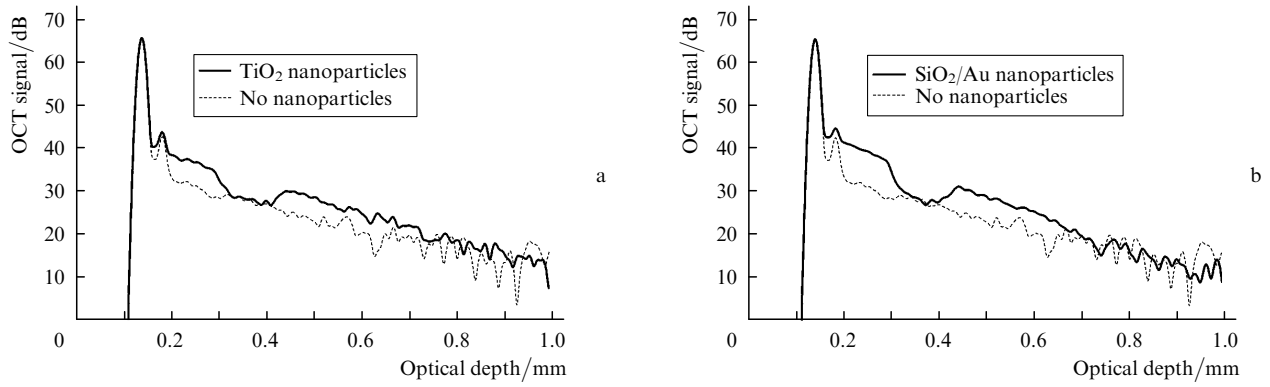

Figure 8. Simulated A-scans along the dashed line in Fig. 7 before and after applying (a) titania and (b) gold nanoshells.

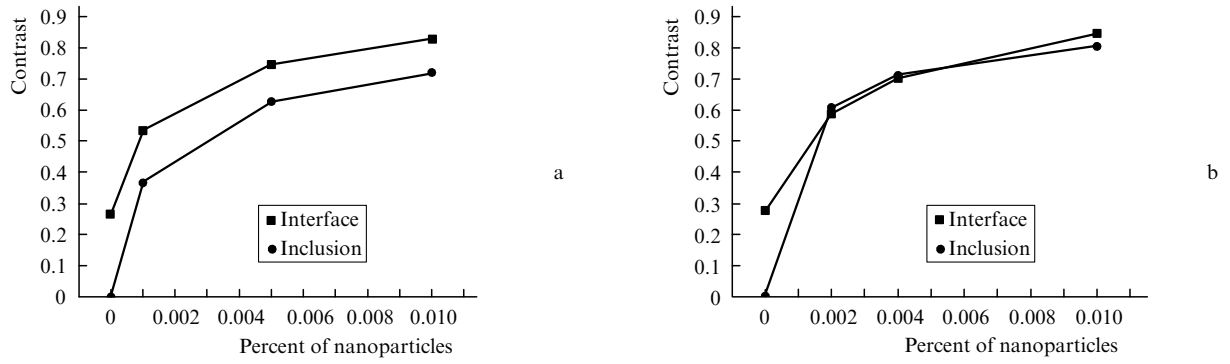

Figure 9. Epidermis–dermis contrast and contrast of inclusions as functions of the volume fraction of (a) titania and (b) gold nanoshells.

4. Conclusions

Both experimental and simulation data demonstrate that nanoparticles enhance the contrast of structural components of skin in OCT imaging. In our experiments with pig skin *in vivo*, the epidermis – dermis contrast was improved from 0.78 ± 0.03 to 0.92 ± 0.04 by gold nanoshells applied to the skin surface and from 0.78 ± 0.03 to 0.86 ± 0.04 by titania nanoparticles. The contrast of glands was enhanced by titania from 0.68 ± 0.12 to 0.84 ± 0.07. In our MC simulations, the contrast of inclusions increased from zero to 0.85 and 0.65, respectively.

We analysed the time variation of imaging contrast and determined the peak contrast time for the skin and nanoparticles studied. The highest contrast in our experiments was reached 120 – 150 min after applying gold nanoparticles and 160 – 200 min after applying titania nanoparticles.

Acknowledgements. This work was supported by the Russian Foundation for Basic Research (Grant Nos 09-02-970040, 10-02-00744, 09-02-00539, 09-02-97072 and 09-02-122156) and the RF President's Grants Council (Grant Nos MK-1127-2010.2 and MD-3018.2009.7).

References

1. Tuchin V.V. (Ed.) *Optical Clearing of Tissues and Blood* (Bellingham: SPIE Press, 2005).
2. *Handbook of Optical Biomedical Diagnostics* (Bellingham: SPIE Press, 2002).
3. Tuchin V.V. (Ed.) *Handbook of Coherent Domain Optical Methods: Biomedical Diagnostics, Environmental and Material Science* (Boston: Kluwer Acad. Publ., 2004).
4. Vo-Dinh T. (Ed.) *Biomedical Photonics Handbook* (Bellingham: SPIE Press, 2003).
5. Bronzino J.D. (Ed.) *The Biomedical Engineering Handbook* (Boca Raton: CRC Press, 2000) Vol. 1, Chap. 61.
6. Bronzino J.D. (Ed.) *The Biomedical Engineering Handbook* (Boca Raton: CRC Press, 2000) Vol. 1, Chap. 63.
7. Collier T., Lacy A., et al. *Acad. Radiology*, **9**, 504 (2002).
8. Bouma B.E., Tearney G.J. (Eds) *Handbook of Optical Coherence Tomography* (New York: Marcel Dekker, 2002).
9. Schmitt J.M. *IEEE J. Sel. Top. Quantum Electron.*, **5** (4), 1205 (1999).
10. Gladkova N.D., Shakhova N.M., Sergeev A.M. (Eds) *Rukovodstvo po opticheskoi kogerentnoi tomografii* (Handbook of Optical Coherence Tomography) (Moscow: Fizmatlit, 2007).
11. Sarvazyan A.P., Skovoroda A.R. *Method and Apparatus for Elasticity Imaging*. Patent US No. 5524636.
12. Zagaynova E.V., Shirmanova M.V., Kirillin M.Yu., Khlebtsov B.N., Orlova A.G., Balalaeva I.V., et al. *Phys. Med. Biol.*, **53**, 4995 (2008).
13. Kirillin M.Yu. et al. *J.Biomed. Opt.*, **14**, 021017 (2009).
14. Troutman T., Barton J.K., Romanowski M. *Opt. Lett.*, **32** (11), 1438 (2007).
15. Zagainova E.V., Shirmanova M.V., Kamensky V.A., Kirillin M.Yu., et al. *Ross. Nanotekhnol.*, **2** (7 – 8), 135 (2007).
16. Kah J.C.Y. et al. *J. Biomed. Opt.*, **14** (5), 054015 (2009).
17. Kuranov R.V., Sapozhnikova V.V., Turchin I.V., Zagainova E.V., Gelikonov V.M., Kamensky V.A., et al. *Opt. Express*, **10**, 707 (2002).
18. Agrba P.D., Kirillin M.Yu., Abelevich A.I., Zagainova E.V., Kamensky V.A. *Opt. Spektrosk.*, **107** (6), 903 (2009).
19. Meglinski I., Kirillin M., Kuzmin V., Myllylä R. *Opt. Lett.*, **33** (14), 1581 (2008).
20. Kirillin M.Yu., Priezzhev A.V., Myllylä R. *Kvantovaya Elektron.*, **38** (6), 570 (2008) [*Quantum Electron.*, **38** (6), 570 (2008)].
21. Tuchin V.V. *Lazery i volokonnaya optika v biomeditsinskikh issledovaniyakh* (Lasers and Fibre Optics in Biomedical Research) (Saratov: Saratovsk. Univ., 1998).
22. Knuttel A., Boehlau-Godau M. *J. Biomed. Opt.*, **5**, 83 (2000).
23. Palik E.D. (Ed.) *Handbook of Optical Constants of Solids* (Orlando: Acad. Press, 1985).
24. Gupta R.P, Wall T.F. *J. Phys. D: Appl. Phys.*, **14**, L95-8 (1981).
25. Johnson P.B., Christy R.W. *Phys. Rev. B*, **6**, 4370 (1972).